Supporting Information:

Stepwise Oxidation of Aqueous Dicarboxylic Acids by Gas-Phase OH-Radicals

Shinichi Enami[a,b,c]*, Michael R. Hoffmann[d] and Agustín J. Colussi[d]*

[a]*The Hakubi Center for Advanced Research, Kyoto University, Kyoto 606-8302, Japan*

[b]*Research Institute for Sustainable Humanosphere, Kyoto University, Uji 611-0011, Japan*

[c]*PRESTO, Japan Science and Technology Agency, Kawaguchi 332-0012, Japan*

[d]*Linde Center for Global Environmental Science, California Institute of Technology, California 91125, U.S.A*

---

*Author to whom correspondence should be addressed: enami.shinichi.3r@kyoto-u.ac.jp or ajcoluss@caltech.edu

SI Text

SI Methods

Ozone is produced from ultrapure O_2(g) (purity > 99.995 %) flowing at 1.0 standard liters per minute through a high-pressure discharge ozonizer (KSQ-050, Kotohira). O_3(g) concentration is quantified online by a UV-Vis absorption spectrophotometry at 250 nm and 300 nm, (absorption cross sections σ = 1.1 x 10^{-17} and 3.9 x 10^{-19} cm^2 $molecule^{-1}$, respectively)[1] prior to entering the reaction chamber (Fig. S1). Throughout, the reported [O_3(g)] values correspond to the concentrations actually sensed by the microjets in the reaction chamber, which are ~10 times smaller than those determined upstream UV absorbances due to dilution by the drying gas. H_2O(g) is carried into the chamber via a known flow of N_2(g) saturated by sparging milli-Q water (Fig. S1). We assume that the chamber is saturated with H_2O(g) at 298 K throughout.

The 266 nm beam emitted by our Nd^{3+}:YAG laser setup (LOTIS TII, LS-2131M-10 with a harmonic generator assembly HG-TF, pulse duration 8 $\pm$ 1 ns, 266 nm beam diameter 10.0 $\pm$ 1.0 mm, beam divergence ≤ 1.5 mrad, 10 Hz) is used to generate ·OH(g) at or near the gas-liquid interface (Fig. S1). The 266 nm laser beam energies are measured with a power meter (OPHIR, NOVA II, sensor:3A-P-V1-ROHS). The 266 nm beam energy is tuned up to 40 mJ $pulse^{-1}$. $[\cdot OH(g)]_0$ can be varied from a few tens of ppbv to 100 ppmv (see [·OH(g)] estimates). Note that $O(^3P)$ may also abstract H-atoms,[2] but with rate constants > 50 times smaller than for ·OH.[3] The fate of $O(^3P)$ is to react with O_2(g) to regenerate O_3 within 50 μs under present conditions.[3] The laser beam is introduced into the spraying chamber via quartz prisms (synthetic fused silica, refractive index n_d = 1.458) on kinematic prism holders (SIGMAKOKI Co., LTD., Japan) and finely aligned with

a He-Ne laser (Melles Griot, 05-LHP-111, 632.8 nm CW) beam, which becomes visible as it is scattered upon hitting the liquid jet.

Experimental conditions were as follows: drying gas flow rate: 12 L min^{-1}; drying gas temperature: 340 ^{o}C; inlet voltage: + 3.5 kV relative to ground; fragmentor voltage value: 80 V. Malonic acid (purity > 99 %), succinic acid (> 99.5 %) and adipic acid (> 99.5 %) were purchased from Nacalai Tesque (Kyoto, Japan). Suberic acid (> 99 %), glutaric acid (> 99 %), pimeric acid (> 98 %) were purchased from Tokyo Chemical Industry Co., Ltd. Oxalic acid (> 99.5 %) and D_2O (99.9 %) were purchased from Sigma-Aldrich. $H_2{}^{18}O$ (97 %) was purchased from Santa Cruz Isotope. All solutions were prepared in purified water (Resistivity ≥ 18.2 MΩ cm at 298 K) from a Millipore Milli-Q water purification system. The pH of solution was measured by a calibrated pH meter, Horiba LAQUA F-74, before the experiments. All experiments were performed at 298 $\pm$ 2 K.

Experimental details

Since mass spectrometers detect net charge, the first step is the separation of pre-existing anions from cations in the inflowing solutions.[4,5]

1- We have demonstrated experimentally that the charges we detect are largely produced pneumatically by showing that ion signals (i) increase at higher gas velocities v_g and (ii) extrapolate to zero as $v_g \rightarrow 0$.[5] The droplets breakup and charge separation mechanisms are shown in elsewhere.[5,6]

2- We have confirmed that the polarizations, if any, of the microjets do not affect the observed chemistries[7-12] by showing that the kinetics of the reaction of dissolved α-tocopherol with gaseous ozone determined on the basis of negative and positive ion detection were identical. [10] We also showed that the titration curves of

carboxylic acids and trimethylamine obtained from the dependence of the carboxylate and trimethylammonium mass spectrometric signals as functions of pH in this setup are unaffected by polarization and identical to those determined by standard titrations in the injected solutions, both leading to the ionization constants reported in the literature, i.e., pKa = 4.8 and 9.8, respectively. [7,8]

3- Since the nebulizer gas can fragment the first generation microdroplets but not the smaller charged droplets for hydrodynamic reasons,[13,14] the creation of net charge is a one-time event. The ejection of dissolved ions to the gas-phase takes place only from the smallest droplets at the end of a sequence of events comprising extensive solvent evaporation, and net charge crowding in shrinking droplets that become unstable and undergo a cascade of Coulomb explosions.[15,16] Finally, gas-phase ions are sorted out and detected by the online mass spectrometer.

4- The concentration dependences observed in present and previous experiments strongly support our assumption that the detected species are indeed produced on the surface of the intact jet containing microdroplets (D_0 > 1 μm) (whose composition is identical to that of the injected solution) rather than on the ensemble of daughter droplets (whose compositions span the broad distributions generated by random solvent evaporation).[7-9,17] This finding corroborates previous reports showing that the titration curves of carboxylic acids and trimethylamine obtained from the dependence of the carboxylate and trimethylammonium mass spectrometric signals as functions of pH in this setup are identical to those determined by standard titrations in the injected solutions. [7,8]

5- The possibility that the species we monitor were produced in the reactions of gases with the highly concentrated, high surface-to-volume small droplets undergoing

Coulomb explosions is excluded by many experimental evidences.[5,8,10,12,17-22] Furthermore, we had found that product signal intensities *decrease* (rather than increase) by injecting the reactive gases 5 mm and 10 mm downstream (relative to the standard position of the gas injector) along the jet direction.[23] This is the expected outcome of a process in which products are formed in collisions of the reactive gases with the intact jet. The fact that product formation is not completely suppressed by shifting the gas injector downstream is ascribed to the fact that the gas beams lose their collimation by turbulent mixing with the nebulizer gas at the reaction zone.

6- Previous data analysis based on mass balances and the kinetic theory of gases[24] suggested that the thickness of the interfacial layers sampled in these experiments is less than one nm.[8,25] More compellingly, we recently demonstrated that the depth of the interfacial layers sampled in our experiments is controllable as a function of nebulizer gas velocity v_g.[5] Under the present high v_g (~160 m/s) condition, anions that reside at the topmost layers of the air–water interface are preferentially detected as mass signals.[5]

$[\cdot OH(g)]_0$ estimates

The dissociation of $O_3(g)$ by 266 nm photons into $O(^1D)$, followed by the reaction of $O(^1D)$ with $H_2O(g)$, in competition with its deactivation by $N_2(g)$ and $O_2(g)$ into $O(^3P)$, promptly yields ·OH(g).[26] We estimate that under our experimental conditions 0.1 ~ 10 % $O_3(g)$ is converted in ·OH(g). The concentration of ·OH hitting the microjet is derived from the $O_3(g)$ absorption cross sections, laser fluence, and reported gas-phase kinetic parameters. Since number of photons is always larger than number of $O_3(g)$ molecules under present conditions, we estimate the initial $O(^1D)$ concentrations from 266 nm photolysis from Beer's law:

$$\ln(N_0/N) = I_0\,\sigma\,\Phi_{dis} \quad \text{(E 1)}$$

$$N = N_0\,exp(-I_0\,\sigma\,\Phi_{dis}) \quad \text{(E 2)}$$

where σ is the absorption cross section, Φ_{dis} is the dissociation quantum yield, I_0 is the laser fluence in number of photons per unit area, N_0 is the number of molecules before laser irradiation, and N is the number of molecules after laser irradiation.[27] $O(^1D)$ reacts with excess $H_2O(g)$ ($[H_2O(g)] \sim 7.6 \times 10^{17}$ molecules cm^{-3}) to form ·OH radical within ~6 ns (from $k_1 = 2.2 \times 10^{-10}$ cm^3 $molecule^{-1}$ s^{-1}), reaction R 1[1,3];

$$O(^1D) + H_2O \rightarrow 2\,\cdot OH \quad \text{(1)}$$

or, is competitively deactivated by N_2 and O_2, reactions R 2a and R 2b

$$O(^1D) + N_2 \rightarrow O(^3P) + N_2 \quad \text{(2a)}$$

$$O(^1D) + O_2 \rightarrow O(^3P) + O_2 \quad \text{(2b)}$$

where $k_{2a} = 2.6 \times 10^{-11}$, $k_{2b} = 4.0 \times 10^{-11}$ cm^3 $molecule^{-1}$ s^{-1}, respectively.[1,3] We estimate that ~ 20 % $O(^1D)$ is converted into ·OH radicals under present conditions. $O(^3P)$ is largely consumed by O_2 to regenerate O_3 ($\tau \sim 36$ μs) under present conditions. In this manner, $[\cdot OH(g)]_0$ can be varied from a few tens of ppbv to 100 ppmv. Note that the reaction of $O(^1D)$ with HOOC-R_n-COOH(aq) is negligible. By assuming a plausible upper limit to the rate constant for such process as large as $k = 6 \times 10^{-10}$ cm^3 $molecule^{-1}$ s^{-1},[28] we estimate that this $O(^1D)$ reaction channel at [HOOC-R_n-COOH] = 0.2 mM = 1.2×10^{17}

molecules cm^{-3}, is still > 10 times slower than the gas phase reactions R1, 2a and 2b. The fact that the same products were observed on aqueous HOOC-R_6-COOH microjets over the 0.01–1.0 mM range also supports it. Importantly, note that even if $O(^1D)$ could survive via reactions R1, 2a and 2b in the gas-phase, $O(^1D)$ will be quantitatively converted into 2 ·OH radicals at the air-water interface where water is in exceedingly large excess over sub-mM DCAs.[18] In other words, the reactions we observe are necessarily driven by ·OH at the air-water interface.

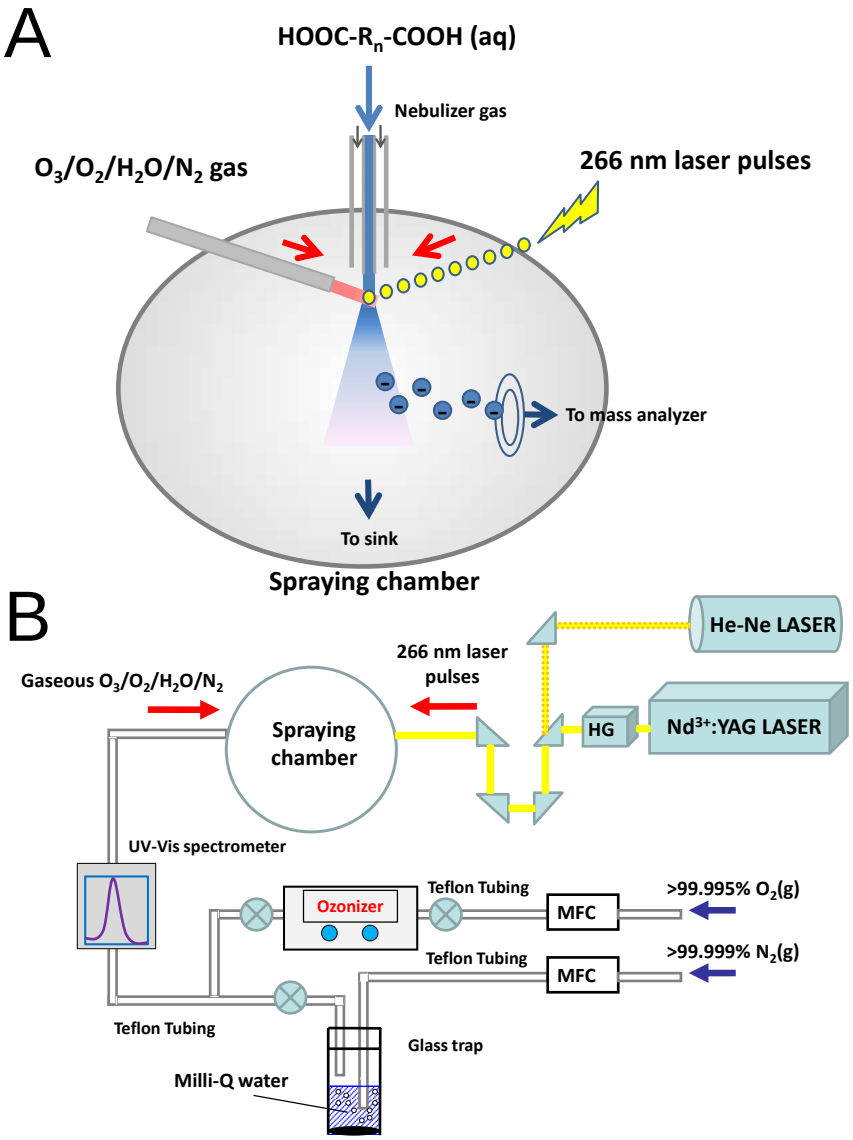

Figure S1 - Schematic diagram of our setup. It allows for the *in-situ* monitoring of reactions of laser-generated gas-phase OH radical on the surface of aqueous solutions. HG stands for harmonic generator, MFC for mass flow controller.

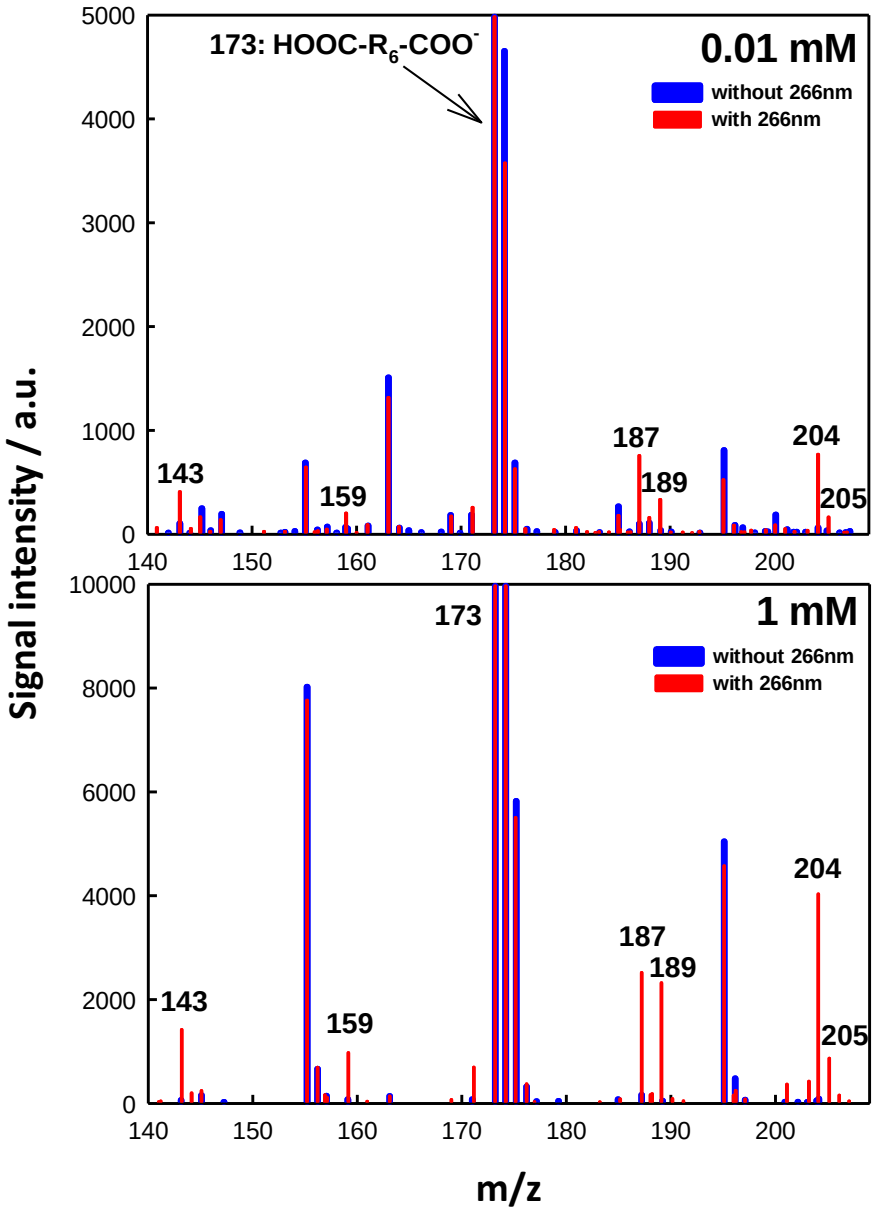

Figure S2 - Negative ion electrospray mass spectra of 0.01 mM (pH 5.3, upper panel) and 1 mM (pH 3.5, lower panel) suberic acid (HOOC-R_6-COOH) microjets exposed to 280 ppmv and 470 ppmv O_3(g), respectively, in O_2(g)/H_2O(g)/N_2(g) mixtures at 1 atm and 298 K. Blue: laser off. Red: under 40 mJ, ~ 8 ns pulses (at 10 Hz) of 266 nm radiation. $[\cdot OH(g)]_0$ ~ 26 ppmv and 44 ppmv, respectively . 1 ppmv = 2.46×10^{13} molecules cm^{-3}.

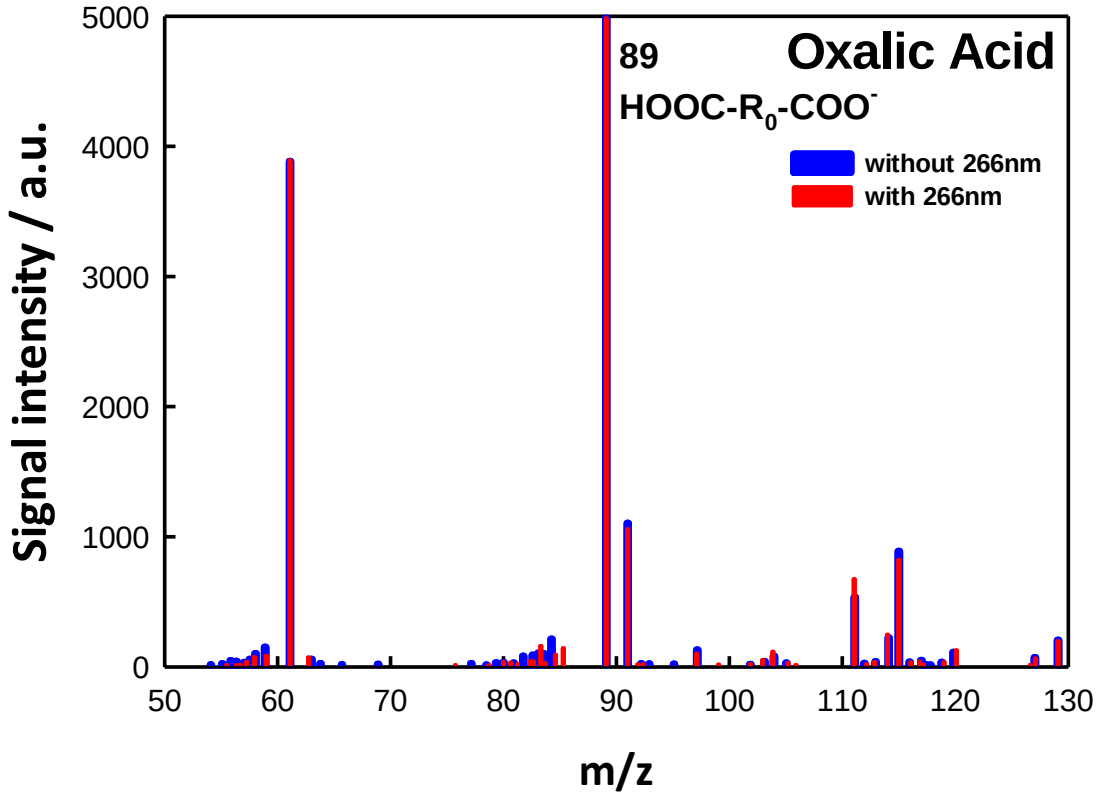

Figure S3 - Negative ion electrospray mass spectra of 10 mM (pH 1.4) oxalic acid (HOOC-R_0-COOH) microjets exposed to 1160 ppmv O_3(g) in O_2(g)/H_2O(g)/N_2(g) mixtures at 1 atm and 298 K. Blue: laser off. Red: under 40 mJ, ~ 8 ns pulses (at 10 Hz) of 266 nm radiation. $[\cdot OH(g)]_0$ ~ 110 ppmv. 1 ppmv = 2.46×10^{13} molecules cm^{-3}.

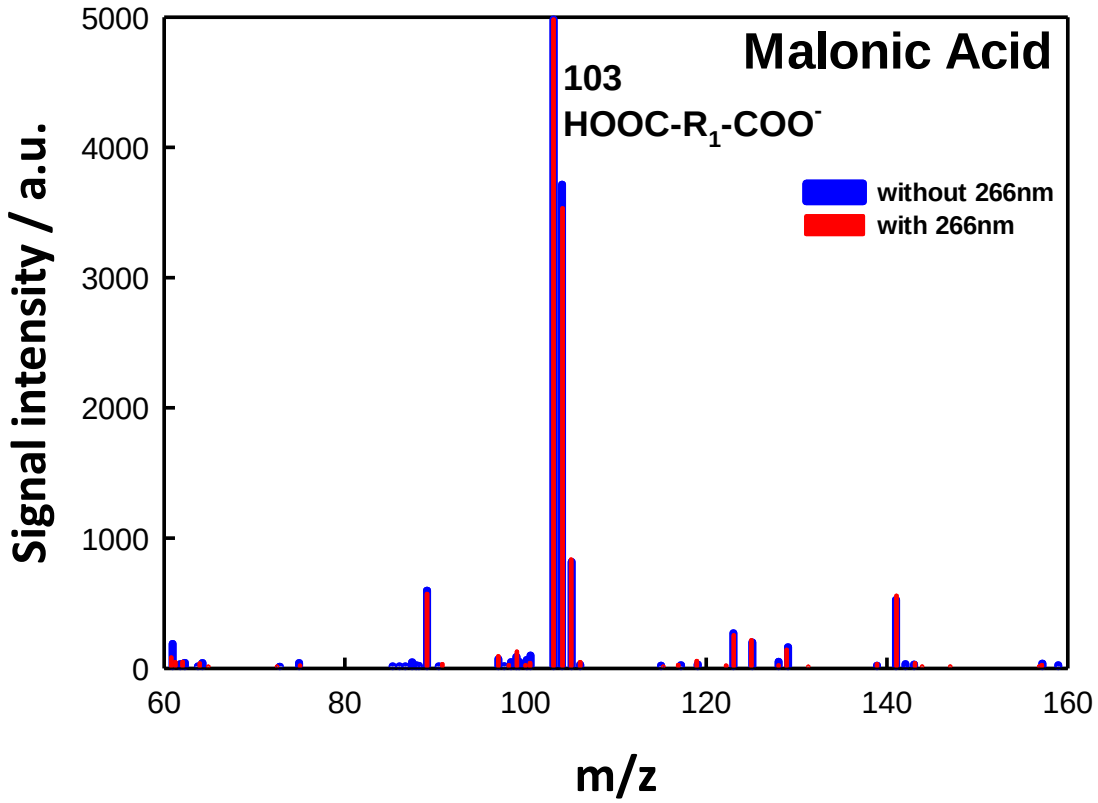

Figure S4 - Negative ion electrospray mass spectra of 10 mM (pH 1.8) malonic acid (HOOC-R_1-COOH) microjets exposed to 970 ppmv O_3(g) in O_2(g)/H_2O(g)/N_2(g) mixtures at 1 atm and 298 K. Blue: laser off. Red: under 40 mJ, ~ 8 ns pulses (at 10 Hz) of 266 nm radiation. $[\cdot OH(g)]_0 \sim 92$ ppmv. 1 ppmv = 2.46×10^{13} molecules cm^{-3}.

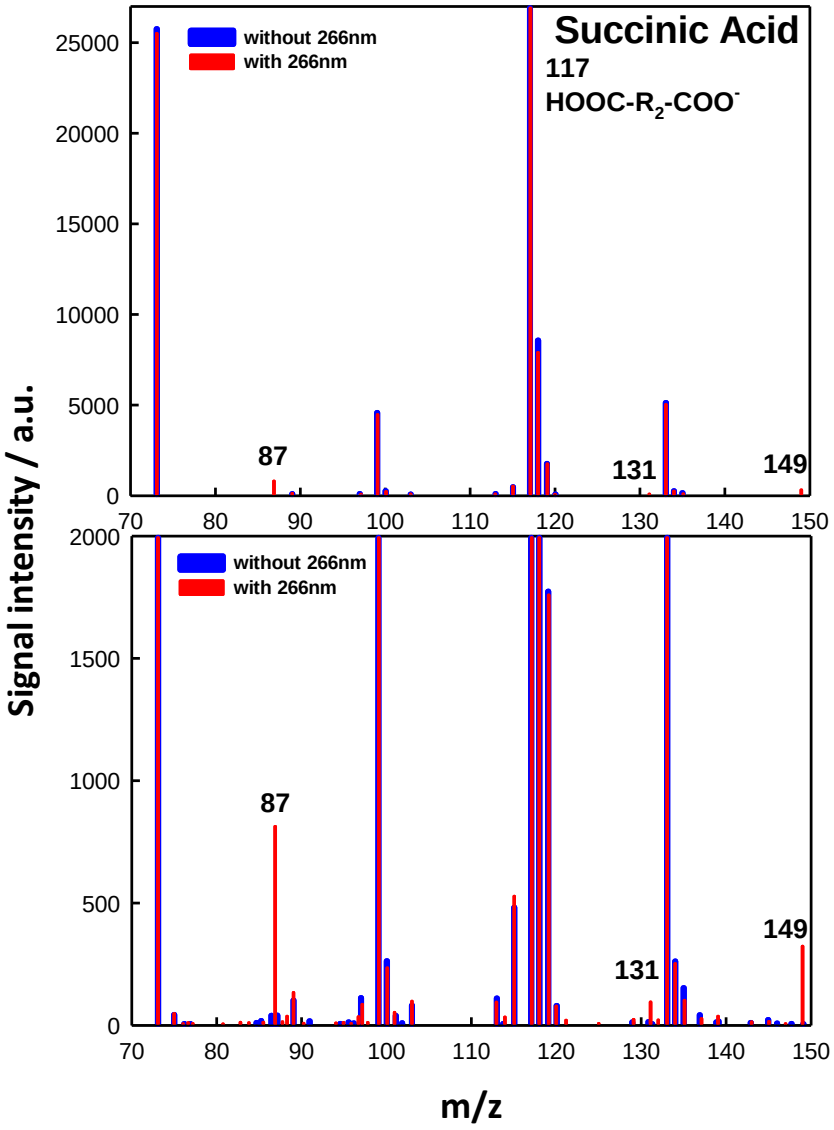

Figure S5 – Upper panel, negative ion electrospray mass spectra of 10 mM (pH 2.6) succinic acid (HOOC-R_2-COOH) microjets exposed to 700 ppmv O_3(g) in O_2(g)/H_2O(g)/N_2(g) mixtures at 1 atm and 298 K. Blue: laser off. Red: under 40 mJ, ~ 8 ns pulses (at 10 Hz) of 266 nm radiation. $[\cdot OH(g)]_0$ ~ 67 ppmv. 1 ppmv = 2.46 × 10^{13} molecules cm^{-3}. The m/z = 87, 131 and 149 is assigned to O=C(H)-R_1-COO^-, HOOC-R_2(-2H)(=O)-COO^- and HOOC-R_2(-H)(OOH)-COO^-, respectively. Lower panel, zooming in spectra of the ·OH-oxidation products.

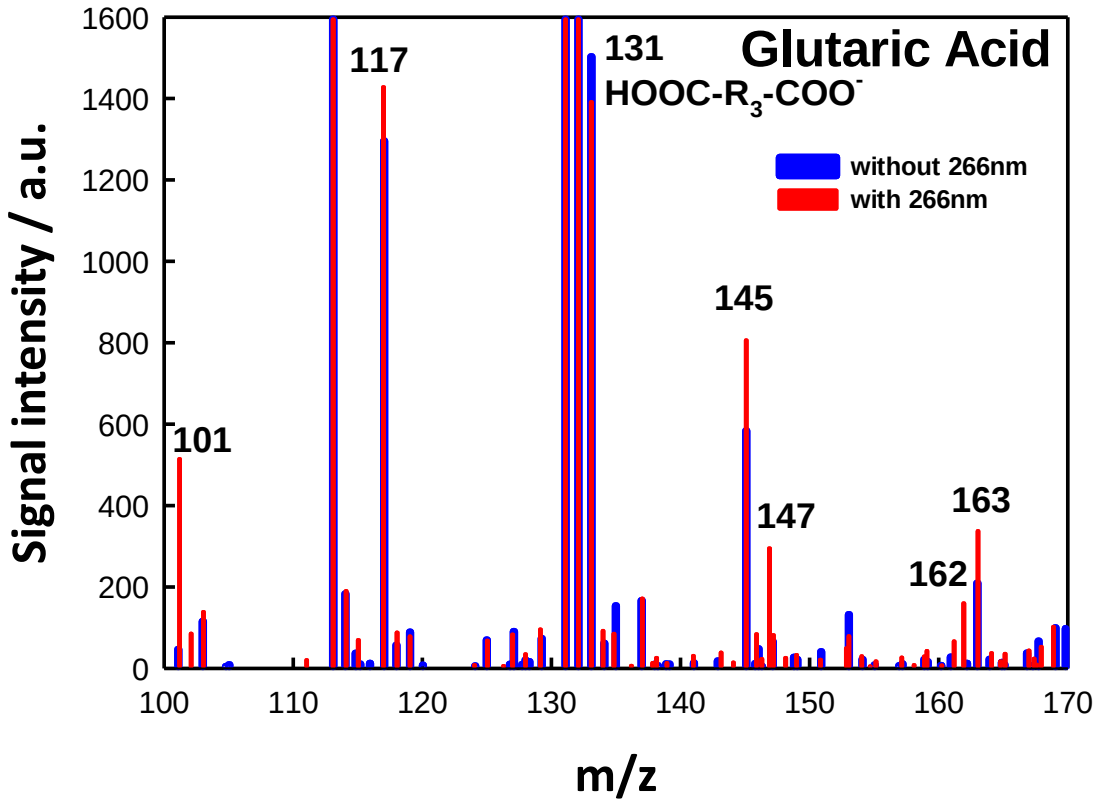

Figure S6 - Negative ion electrospray mass spectra of 1 mM (pH 3.8) glutaric acid (HOOC-R_3-COOH) microjets exposed to 100 ppmv O_3(g) in O_2(g)/H_2O(g)/N_2(g) mixtures at 1 atm and 298 K. Blue: laser off. Red: under 40 mJ, ~ 8 ns pulses (at 10 Hz) of 266 nm radiation. $[\cdot OH(g)]_0$ ~ 10 ppmv. 1 ppmv = 2.46 × 10^{13} molecules cm^{-3}. The m/z = 101, 117, 145, 147, 162 and 163 is assigned to O=C(H)-R_2-COO^-, HOOC-R_2-COO^-, HOOC-R_3(-2H)(=O)-COO^-, HOOC-R_3(-H)(OH)-COO^-, HOOC-R_3(-H)(OO·)-COO^- and HOOC-R_3(-H)(OOH)-COO^-, respectively.

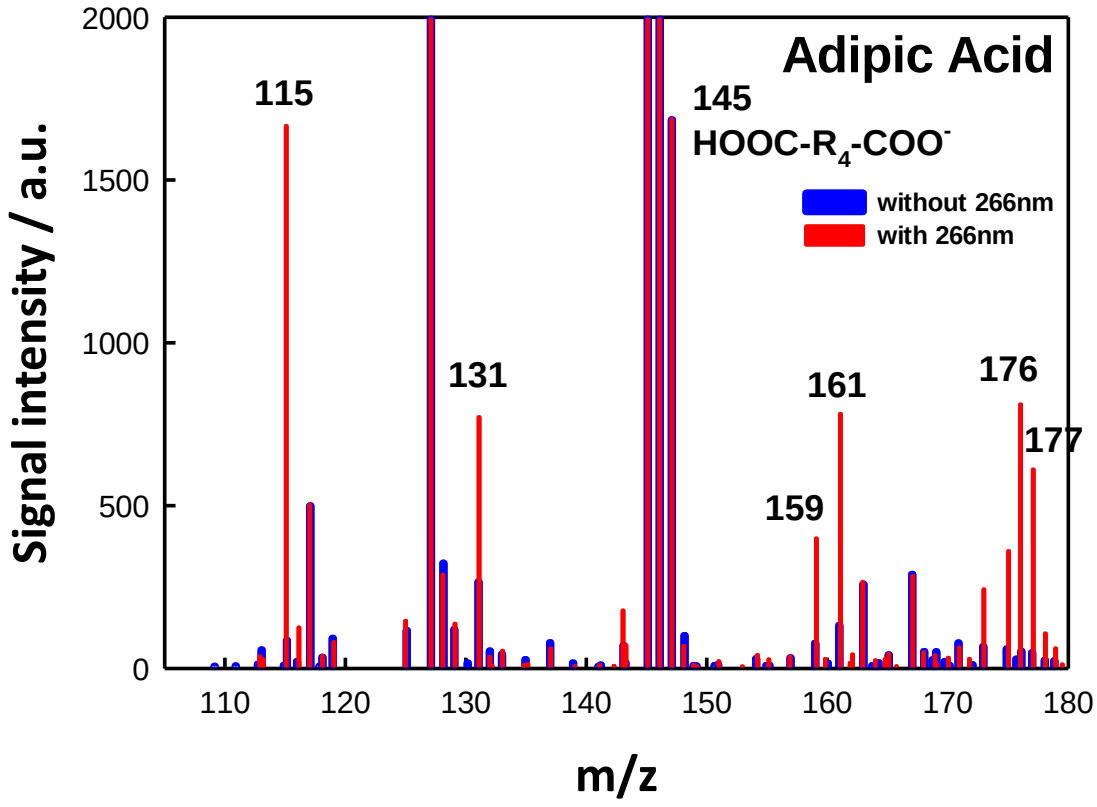

Figure S7 - Negative ion electrospray mass spectra of 1 mM (pH 3.7) adipic acid (HOOC-R_4-COOH) microjets exposed to 660 ppmv O_3(g) in O_2(g)/H_2O(g)/N_2(g) mixtures at 1 atm and 298 K. Blue: laser off. Red: under 40 mJ, ~ 8 ns pulses (at 10 Hz) of 266 nm radiation. $[\cdot OH(g)]_0$ ~ 63 ppmv. 1 ppmv = 2.46 × 10^{13} molecules cm^{-3}. The m/z = 115, 131, 159, 161, 176 and 177 is assigned to O=C(H)-R_3-COO^-, HOOC-R_3-COO^-, HOOC-R_4(-2H)(=O)-COO^-, HOOC-R_4(-H)(OH)-COO^-, HOOC-R_4(-H)(OO·)-COO^- and HOOC-R_4(-H)(OOH)-COO^-, respectively.

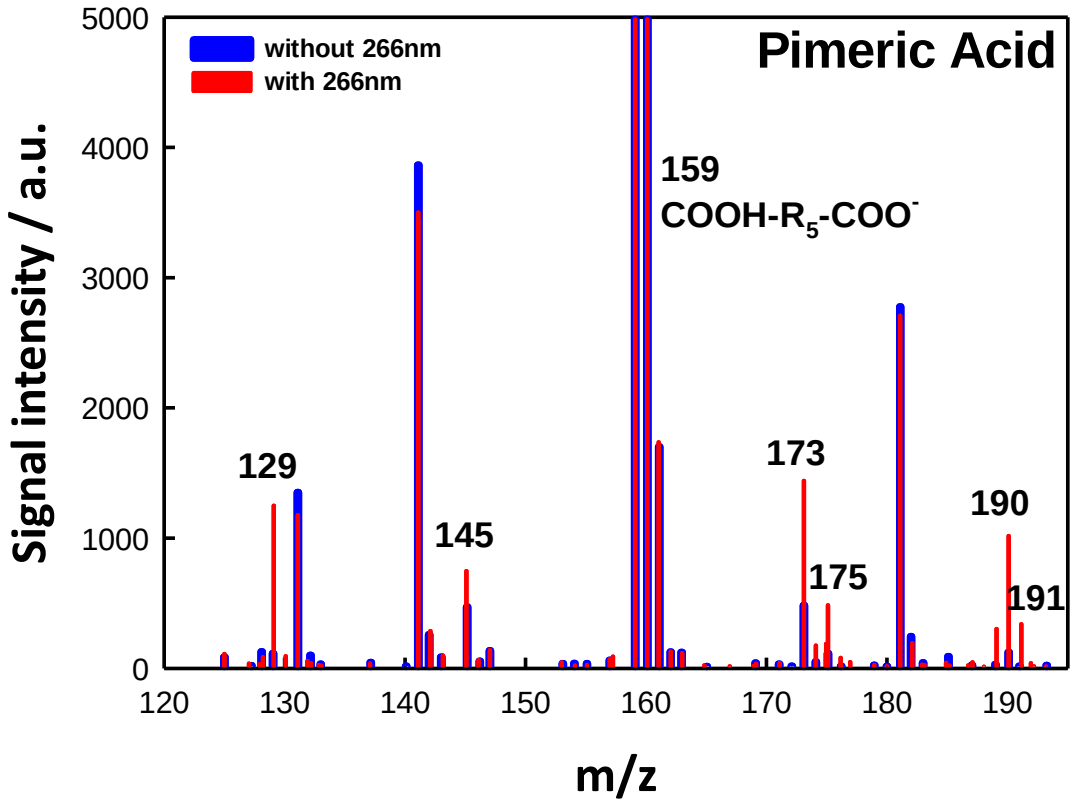

Figure S8 - Negative ion electrospray mass spectra of 1 mM (pH 3.8) pimeric acid (HOOC-R_5-COOH) microjets exposed to 1150 ppmv O_3(g) in O_2(g)/H_2O(g)/N_2(g) mixtures at 1 atm and 298 K. Blue: laser off. Red: under 40 mJ, ~ 8 ns pulses (at 10 Hz) of 266 nm radiation. $[\cdot OH(g)]_0$ ~ 109 ppmv. 1 ppmv = 2.46 × 10^{13} molecules cm^{-3}. The m/z = 129, 145, 173, 175, 190 and 191 is assigned to O=C(H)-R_4-COO^-, HOOC-R_4-COO^-, HOOC-R_5(-2H)(=O)-COO^-, HOOC-R_5(-H)(OH)-COO^-, HOOC-R_5(-H)(OO·)-COO^- and HOOC-R_5(-H)(OOH)-COO^-, respectively.

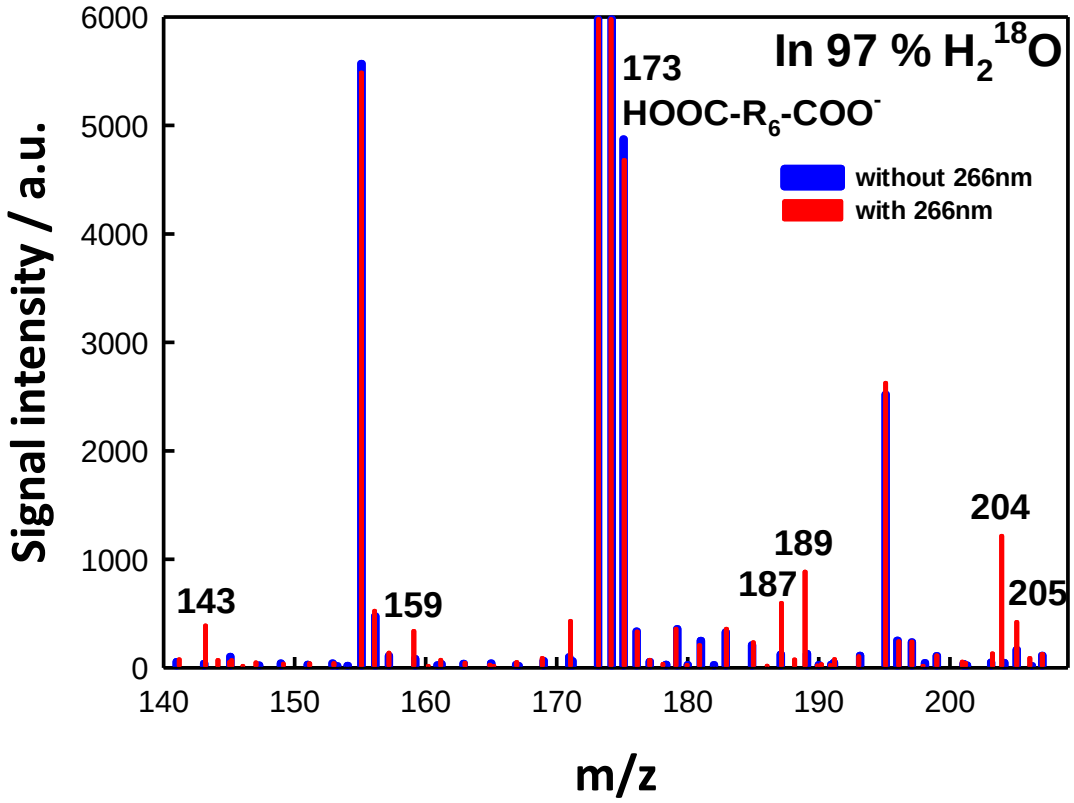

Figure S9 - Negative ion electrospray mass spectra of 0.7 mM suberic acid (HOOC-R_6-COOH) in 97 % $H_2{}^{18}O$ microjets exposed to 270 ppmv O_3(g) in O_2(g)/H_2O(g)/N_2(g) mixtures at 1 atm and 298 K. Blue: laser off. Red: under 40 mJ, ~ 8 ns pulses (at 10 Hz) of 266 nm radiation. $[\cdot OH(g)]_0$ ~ 25 ppmv. 1 ppmv = 2.46×10^{13} molecules cm^{-3}. The m/z = 143, 159, 187, 189, 204 and 205 is assigned to O=C(H)-R_5-COO^-, HOOC-R_5-COO^-, HOOC-R_6(-2H)(=O)-COO^-, HOOC-R_6(-H)(OH)-COO^-, HOOC-R_6(-H)(OO·)-COO^- and HOOC-R_6(-H)(OOH)-COO^-, respectively.

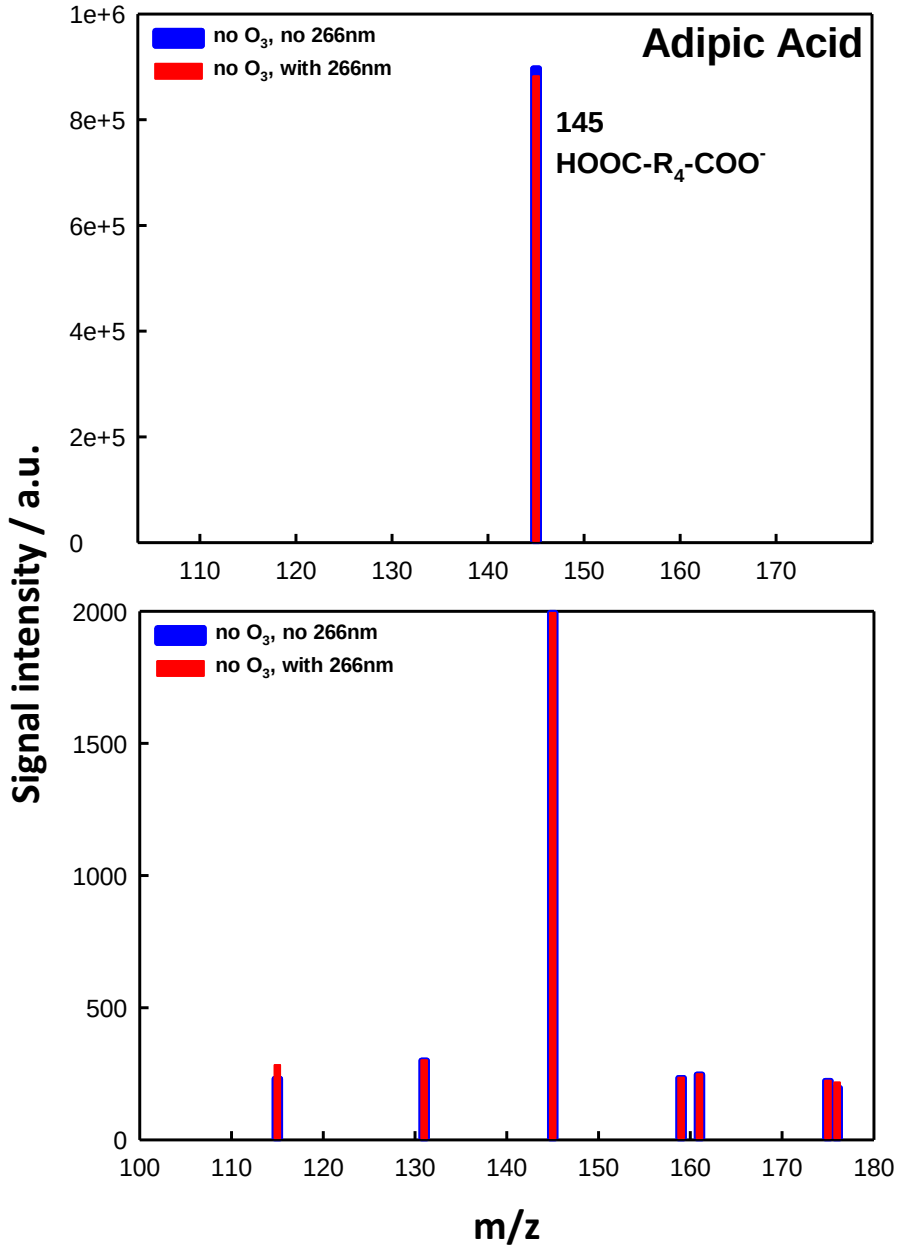

Figure S10 – A) Negative ion electrospray mass spectra of 1 mM adipic acid (HOOC-R_4-COOH) microjets measured by selective ion mode for the reactant and possible products signals in the absence (blue)/presence (red) of 266 nm laser beam irradiation at 40 mJ $pulse^{-1}$ (maximum power) under $H_2O/O_2/N_2$ atmosphere. B) Zooming in spectra in the 100 - 180 Da range.

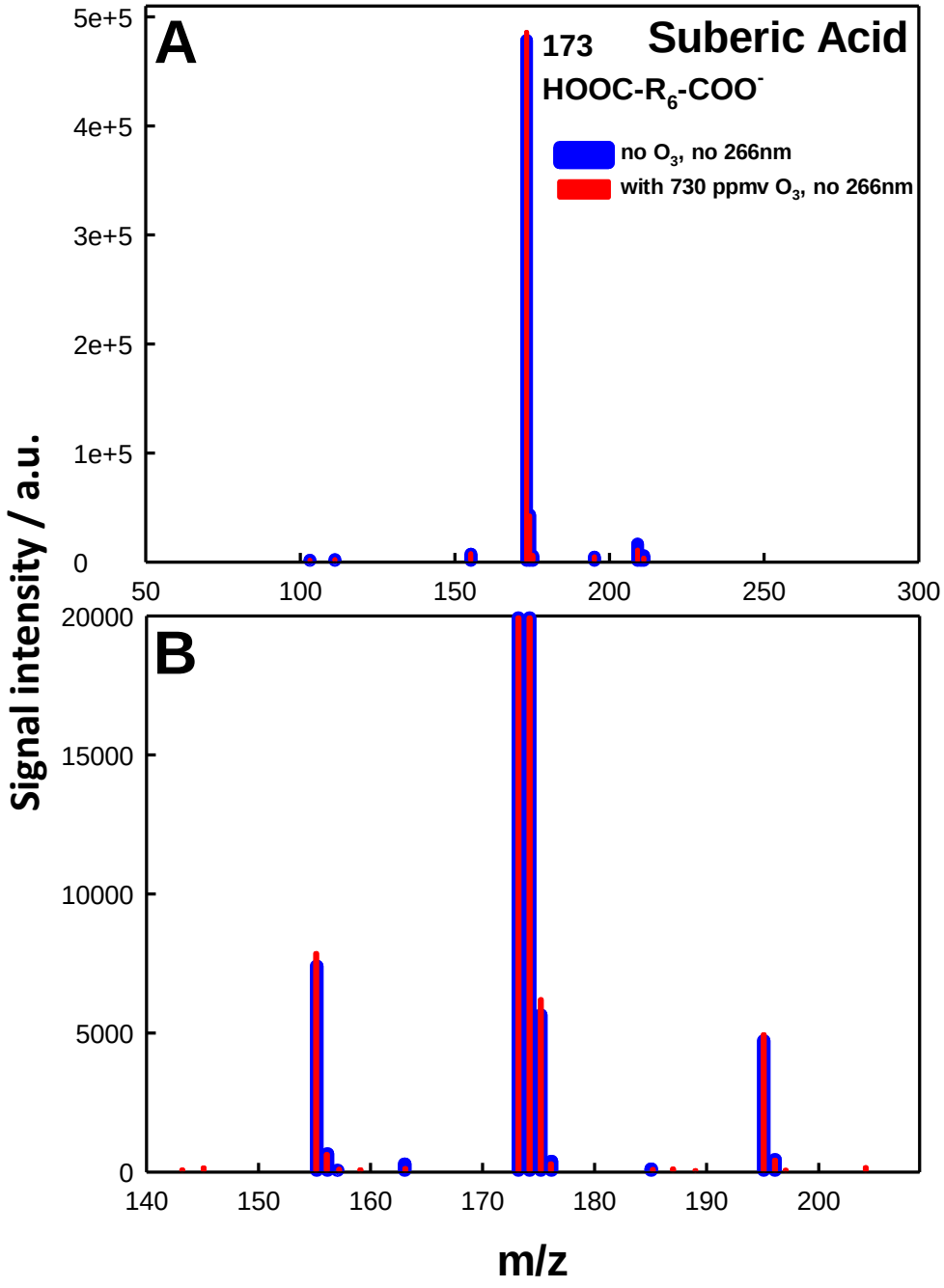

Figure S11 – A) Negative ion electrospray mass spectra of 1 mM suberic acid (HOOC-R_6-COOH) microjets in the absence (blue)/presence (red) of 730 ppmv O_3(g) in $H_2O/O_2/N_2$ atmosphere under no 266 nm irradiation. B) Zooming in spectra in the 140 – 210 Da range.

SI REFERENCES

(1) Sander, S. P.; Friedl, R. R.; DeMore, W. B.; Ravishankara, A. R.; Golden, D. M.; Kolb, C. E.; Kurylo, M. J.; Hampson, R. F.; Huie, R. E.; Molina, M. J.et al. *Chemical Kinetics and Photochemical Data for Use in Stratospheric Modeling Supplement to Evaluation 12: Update of Key Reactions Evaluation Number 13*, 2000.

(2) Waring, C.; Bagot, P. A. J.; Costen, M. L.; McKendrick, K. G. Reactive Scattering as a Chemically Specific Analytical Probe of Liquid Surfaces. *J. Phys. Chem. Lett.* **2011**, *2*, 12-18.

(3) National Institute of Standards and Technology Standard Reference Database Number 69. **2009**.

(4) Enami, S.; Colussi, A. J. Long-range Hofmeister effects of anionic and cationic amphiphiles. *J. Phys. Chem. B* **2013**, *117*, 6276-6281.

(5) Enami, S.; Colussi, A. J. Long-range specific ion-ion interactions in hydrogen-bonded liquid films. *J. Chem. Phys* **2013**, *138*, 184706.

(6) Zilch, L. W.; Maze, J. T.; Smith, J. W.; Ewing, G. E.; Jarrold, M. F. Charge separation in the aerodynamic breakup of micrometer-sized water droplets. *J. Phys. Chem. A* **2008**, *112*, 13352-13363.

(7) Mishra, H.; Enami, S.; Nielsen, R. J.; Stewart, L. A.; Hoffmann, M. R.; Goddard, W. A.; Colussi, A. J. Bronsted basicity of the air-water interface. *Proc. Natl. Acad. Sci. U.S.A.* **2012**, *109*, 18679-18683.

(8) Enami, S.; Hoffmann, M. R.; Colussi, A. J. Proton Availability at the Air/Water Interface. *J. Phys. Chem. Lett.* **2010**, *1*, 1599-1604.

(9) Enami, S.; Hoffmann, M. R.; Colussi, A. J. Acidity enhances the formation of a persistent ozonide at aqueous ascorbate/ozone gas interfaces. *Proc. Natl. Acad. Sci. U.S.A.* **2008**, *105*, 7365-7369.

(10) Enami, S.; Hoffmann, M. R.; Colussi, A. J. How phenol and alpha-tocopherol react with ambient ozone at gas/liquid interfaces. *J. Phys. Chem. A* **2009**, *113*, 7002-7010.

(11) Enami, S.; Vecitis, C. D.; Cheng, J.; Hoffmann, M. R.; Colussi, A. J. Electrospray mass spectrometric detection of products and short-lived intermediates in aqueous aerosol microdroplets exposed to a reactive gas. *J. Phys. Chem. A* **2007**, *111*, 13032-13037.

(12) Enami, S.; Sakamoto, Y.; Colussi, A. J. Fenton chemistry at aqueous interfaces. *Proc. Natl. Acad. Sci. U. S. A.* **2014**, *111*, 623-628.

(13) Lasheras, J. C.; Villermaux, E.; Hopfinger, E. J. Break-up and atomization of a round water jet by a high-speed annular air jet. *J Fluid Mech* **1998**, *357*,

351-379.

(14) Gorokhovski, M. A.; Saveliev, V. L. Analyses of Kolmogorov's model of breakup and its application into Lagrangian computation of liquid sprays under air-blast atomization. *Phys Fluids* **2003**, *15*, 184-192.

(15) Iribarne, J. V.; Thomson, B. A. On the evaporation of small ions from charged droplets. *J. Chem. Phys.* **1976**, *64*, 2287.

(16) Kebarle, P.; Peschke, M. On the mechanisms by which the charged droplets produced by electrospray lead to gas phase ions. *Anal. Chim. Acta* **2000**, *406*, 11.

(17) Mishra, H.; Enami, S.; Nielsen, R. J.; Hoffmann, M. R.; Goddard, W. A.; Colussi, A. J. Anions Dramatically Enhance Proton Transfer through Water Interfaces. *Proc. Natl. Acad. Sci. U .S. A.* **2012**, *109*, 10228-10232.

(18) Enami, S.; Hoffmann, M. R.; Colussi, A. J. In Situ Mass Spectrometric Detection of Interfacial Intermediates in the Oxidation of RCOOH(aq) by Gas-Phase OH-Radicals. *J. Phys. Chem. A* **2014**, *118*, 4130-4137.

(19) Mishra, H.; Enami, S.; Nielsen, R. J.; Stewart, L. A.; Hoffmann, M. R.; Goddard, W. A.; Colussi, A. J. Bronsted basicity of the air-water interface. *Proc. Nat. Acad. Sci. U. S. A.* **2012**, *109*, 18679-18683.

(20) Enami, S.; Hoffmann, M. R.; Colussi, A. J. Dry Deposition of Biogenic Terpenes via Cationic Oligomerization on Environmental Aqueous Surfaces. *J. Phys. Chem. Lett.* **2012**, *3*, 3102-3108.

(21) Enami, S.; Hoffmann, M. R.; Colussi, A. J. Molecular Control of Reactive Gas Uptake "on Water". *J. Phys. Chem. A* **2010**, *114*, 5817-5822.

(22) Enami, S.; Hoffmann, M. R.; Colussi, A. J. Acidity enhances the formation of a persistent ozonide at aqueous ascorbate/ozone gas interfaces. *Proc. Natl. Acad. Sci. U. S. A.* **2008**, *105*, 7365-7369.

(23) Enami, S.; Vecitis, C. D.; Cheng, J.; Hoffmann, M. R.; Colussi, A. J. Global inorganic source of atmospheric bromine. *J. Phys. Chem. A* **2007**, *111*, 8749-8752.

(24) Davidovits, P.; Kolb, C. E.; Williams, L. R.; Jayne, J. T.; Worsnop, D. R. Mass accommodation and chemical reactions at gas-liquid interfaces. *Chem. Rev.* **2006**, *106*, 1323-1354.

(25) Enami, S.; Stewart, L. A.; Hoffmann, M. R.; Colussi, A. J. Superacid Chemistry on Mildly Acidic Water. *J. Phys. Chem. Lett.* **2010**, *1*, 3488-3493.

(26) Grebenshchikov, S. Y.; Qu, Z. W.; Zhu, H.; Schinke, R. New theoretical investigations of the photodissociation of ozone in the Hartley, Huggins, Chappuis, and Wulf bands. *Phys. Chem. Chem. Phys.* **2007**, *9*, 2044-2064.

(27) Lin, J. J.; Chen, A. F.; Lee, Y. T. UV Photolysis of ClOOCl and the Ozone

Hole. *Chemistry-an Asian J.* **2011**, *6*, 1664-1678.

(28) Dillon, T. J.; Horowitz, A.; Crowley, J. N. The atmospheric chemistry of sulphuryl fluoride, SO2F2. *Atmos. Chem. Phys.* **2008**, *8*, 1547-1557.